

LOW-COMPLEXITY DIGITAL FILTER BANK FOR STRONGLY ABERRATED OPTICAL SYSTEMS HAVING VARIABLE F-NUMBERS

Guotong Feng, M. Dirk Robinson, and Kathrin Berkner

Ricoh Innovations, Inc.
2882 Sand Hill Road Suite 115
Menlo Park, CA 94025, USA
E-mail: {feng, dirkr, berkner}@rii.ricoh.com

ABSTRACT

It has been shown that electro-optical imaging systems designed by integrating optics and digital processing provide system-level advantages such as extended depth-of-field and lower optical component costs. In such imaging systems, the strength of the optical aberration or blur can dramatically change with the f-number, and hence different digital filters in the subsequent digital processing are required to correct the captured images at different f-numbers. However, implementing such number of filters in hardware requires expensive computational resources, which in turn increase the overall system cost. In this paper, we propose a simple image filtering approach which uses a weighted sum of a set of component finite impulse response (FIR) filters to effectively apply a different composite FIR filter for each f-number. The simulation results demonstrate that our approach achieves desirable image quality for variable f-numbers, while substantially reducing the complexity in hardware implementation.

Index Terms— Electro-optical imaging, filter bank, FIR, sharpening, spherical aberration, extended depth-of-field, wavefront coding

1. INTRODUCTION

Modern electro-optical imaging systems include imaging optics, sensors, and digital image processors. In traditional design, these subsystems have been optimized in a sequential fashion. First, the optical subsystem is designed to maximize the optical image quality at the focal plane (minimize blur). Second, the digital image processing system is designed to correct any residual artifacts in the digital image captured at the sensor. Recent research demonstrates the advantage of an end-to-end design perspective wherein both the optics and the digital processing subsystems are designed *jointly* [1][2][3][4]. Imaging systems designed in this fashion, which we call jointly designed imaging system, have superior system-level qualities such as extended depth-of-field, better optical sensitivity, and lower component costs [4]. Optical

subsystems produced by this joint design methodology differ from conventional optical systems in that they typically contain large optical aberrations and thereby produce blurry images. Subsequent digital processing is required for such imaging systems to restore the image to the desirable level of image quality.

The amount of blur in an optical image is characterized by the optical system's point spread function (PSF), which is a function of the optical aberrations [5]. The optical image is sampled to create a digital image at the sensor (e.g. CCD) where the sampling is typically uniform. Assuming the optical system PSF is spatially invariant, the image observation model of such imaging systems can be represented by

$$v(m, n) = h(m, n, \Phi) \circledast u(m, n) + \eta(m, n) \quad (1)$$

where h represents the impulse response of the sampled system, \circledast the spatial convolution operator, $u(m, n)$ the sampled original image (i.e. ideal image), $v(m, n)$ the sampled observed image, and $\eta(m, n)$ the detector noise with variance σ^2 . The impulse response h depends on the strength of the optical aberrations, denoted by Φ , which is represented by the vector of the wavefront aberration coefficients [5]. Typically, Φ contains the coefficients of defocus and the third-order or Seidel aberrations, including spherical aberration, coma, astigmatism, field curvature, and distortion. In this paper, we will be only focusing on the systems dominated by spherical aberration with W_{040} being its coefficient in the wavefront aberration function [5]. In traditionally designed systems, the spherical aberration is relatively small (e.g. $W_{040} < 0.5$ wave) because it has already been minimized during the optical design stage. In contrast, in the jointly designed systems analyzed in this paper, the spherical aberration can be significantly larger (e.g. $W_{040} = 7$ waves). Subsequently, such systems require digital sharpening of the observed image to restore the contrast loss due to aberrated optics. Typically, the image processing is represented by a spatially invariant digital filter having a frequency response R which ideally is either an inverse filter, or a Wiener filter [6]. The Wiener filter

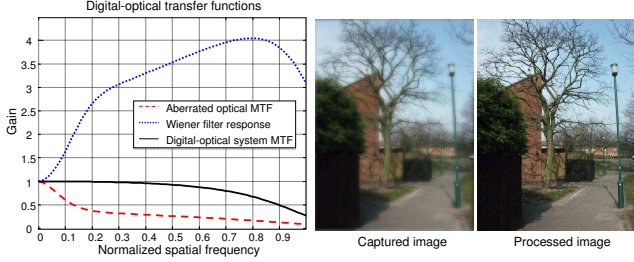


Fig. 1. The left graph shows the optical system MTF (dashed curve), the Wiener filter frequency response (dotted), and the digital-optical system MTF (solid). The center and right graphs show the images before and after being processed by the filter.

frequency response is given by

$$R(\omega, \nu) = \frac{P_s(\omega, \nu)H^*(\omega, \nu)}{P_s(\omega, \nu)|H(\omega, \nu)|^2 + \sigma^2} \quad (2)$$

where $P_s(\omega, \nu)$ is the power spectral density (PSD) of the unknown image signal [6], and $H(\omega, \nu)$ is the optical transfer function (OTF). The Wiener filter minimizes the mean-square-error (MSE) of the estimated signal. The MSE is defined by

$$E_{mse}(H, R) = \int_{\omega} \int_{\nu} P_s(\omega, \nu) |H(\omega, \nu)R(\omega, \nu) - 1|^2 + \sigma^2 |R(\omega, \nu)|^2 d\omega d\nu \quad (3)$$

Fig. 1 shows an example of the electro-optical systems with strong spherical aberration and compensating image processing. The dotted curve in the left graph of Fig. 1 shows the frequency response of a Wiener filter designed for the modulation transfer function (MTF) shown as the dashed curve. The optical MTF of this system is poor (low) relative to traditional optical systems due to significant spherical aberration. The center graph in Fig. 1 shows an example of a blurry image produced by the optical system with such a poor MTF. After applying the Wiener filter, the combined digital-optical system MTF is shown as the solid line in the left graph of Fig. 1. This system MTF is improved considerably with restored contrast as evidenced by the processed image in the right graph of Fig. 1.

Many optical systems offer variable f-numbers such as zoom and aperture settings. Unlike traditionally designed systems, changing the f-number of an electro-optical system can change the OTF so dramatically that different sharpening filters in the subsequent digital processing are required to correct the captured image at different f-numbers. Let Φ_i denote the aberration coefficients of the optical system at a different f-number setting i , where $i = 1, 2, \dots, N$. Correspondingly, the OTF H and the filter frequency response R in (2) and (3) become H_i and R_i respectively. Because the size of

the digital filters is so large, storing digital filters for all the possible states is prohibitively expensive for hardware image processors. We propose an efficient method for minimizing the hardware complexity while achieving high system performance using a specially optimized filter bank. In Sec. 2 we describe the filter-bank architecture and how we optimize the filter bank. In Sec. 3 we show some simulated results for the proposed architecture demonstrating the ability to produce high-quality images at low hardware complexity. Finally, we make conclusions in Sec. 4.

2. OPTIMAL FILTER BANK DESIGN

Varying the f-numbers for aberrated electro-optical imaging systems can induce significant fluctuation in the optical PSF and hence the MTF. For example, Fig. 2 shows an example of optical MTFs ($H_i(\omega, \nu)$, $i = 1, 2, 3$) for a system containing significant spherical aberration as the f-number is varied through three settings $F\# 4.3$, $F\# 3.3$ and $F\# 2.8$. Variation in the MTF of this type requires a set of digital filters with frequency response $\{R_i(\omega, \nu)\}$ for each f-number.

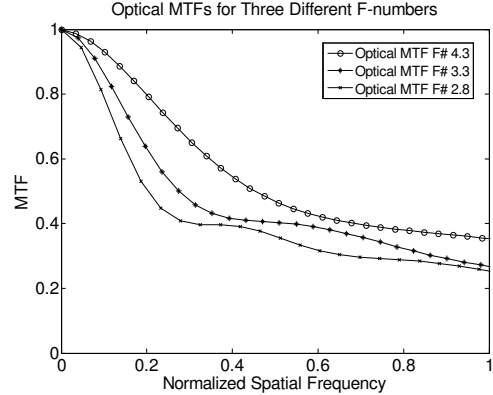


Fig. 2. Optical MTFs for an aberrated system having three f-numbers.

Storing such a set of filters in the digital processing unit, three in this example, is prohibitively costly. Instead, we propose a filter bank approach where the final filter response is given by a linear combination of finite impulse response (FIR) filter kernels

$$R_i(\omega, \nu) = \sum_{k=1}^K \alpha_{ik} F_k(\omega, \nu) \quad (4)$$

where the terms α controls the linear weighting of the set of K filter kernels having a frequency response $F_k(\omega, \nu)$, $k = 1, 2, \dots, K$. The filter response $F_k(\omega, \nu)$ depends on the set of filter kernel coefficients in the spatial domain denoted by $\{f_k\}$. The collection of all the filter kernels are independent of the f-number settings. The weighting terms α_{ik} are chosen depending on the f-number state of the optical system. We

denote the collection of all filter tap kernels and weighting coefficients in vector notation as \mathbf{f} and \mathbf{a} respectively.

Ideally, the set of filter kernels require significantly less computational resources than the naive approach of storing and implementing a set of filter for each state. The simple approach is to use a small set of component filter kernels for a larger set of optical states. Another approach involves using *nested* filter kernels. Fig. 3 shows a block diagram example of such nested filter kernels.

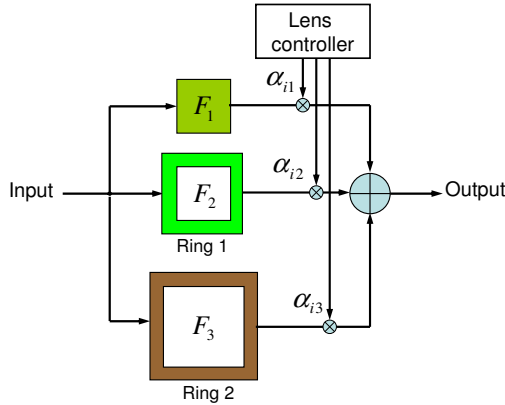


Fig. 3. The block diagram shows an example of a filter bank having a nested structure where the different filter kernels have no overlap in the spatial domain.

In this example, the filter bank consists of three filters including a basic square filter kernel and two other non-overlapping concentric ring filters. The relationship between f-number and PSF size motivates this nested filter structure. As the f-number gets smaller the size of the PSF increases due to the optical aberration. Thus, the effective filter size required to restore the image increases as the f-number decreases. Filter kernels designed in this nested fashion minimize the complexity associated with each of the filter kernels by minimizing the number of multiplications required for each kernel. Also, if we optimize the weighting coefficients α_{ik} such that certain coefficients are zero, then we can save circuit power by turning off entire filter kernels. Finally, the filter bank approach simplifies the hardware implementation of the filters as the individual filter kernels may be implemented without requiring complicated control circuitry to swap filter coefficients in and out of memory or to compute filter coefficients on-the-fly.

Unlike traditional filter banks, the filter kernels comprising the filter bank need not be orthogonal. Of course, in the case of nested filter banks, the kernels are naturally orthogonal in the spatial domain due to their non-overlapping property. Designing filter bank kernels requires non-convex optimization. We design our filter bank kernels according to a minimum MSE criterion over the collection of optical states

according to

$$\min_{\mathbf{f}, \mathbf{a}} \sum_{i=1}^N E_{mse}(H_i, R_i(\mathbf{a}, \mathbf{f})) \quad (5)$$

where E_{mse} represents the MSE given by (3). We implement the filter bank optimization by implicitly constraining the filter geometry by way of construction of the filter tap coefficient variables \mathbf{f} depending on the filter bank properties (e.g. non-overlapping property for the nested filter bank). For spherical aberration dominant systems, the rotational symmetry in the filter kernels can also be exploited to largely reduce the dimension of the parameters to be optimized. The cost function of (5) is non-convex because of the interaction between the weighting terms \mathbf{a} and the filter tap coefficients \mathbf{f} . Consequently, we rely on an optimization routine in Matlab called “fminsearch”. This function applies a simplex search method proposed in [7]. While slow, this optimization approach provides reasonable performance as we will demonstrate in our next section.

3. EXPERIMENTAL RESULTS

We demonstrate the effectiveness of the filter bank approach to correcting variable f-number aberrated optics for the example shown in Fig. 2. In this example, the nested filter bank is comprised of three filter kernels: a 7×7 square center filter, a 9×9 nested square annulus filter, and an 11×11 nested square annulus filter. We optimize both the filter kernel coefficients \mathbf{f} and the state weighting variables \mathbf{a} based on the cost function of (5). We use a very simple model for the PSD function used in (2) based on the adjacent pixel correlation model with correlation coefficient 0.85 as suggested in [6]. The signal-to-noise-ratio (SNR) is assumed to be 40 dB. The $F\#$ 4.3 state has the smallest aperture among the three, suffers from the least amount of spherical aberration, and therefore requires the smallest size composite filter using only one filter kernel. At the other extreme, $F\#$ 2.8 suffers from the most spherical aberration, and therefore requires the largest size composite filter using all three filters kernels.

Fig. 4 shows the frequency responses of the FIR Wiener filters optimized for f-numbers: $F\#$ 4.3, $F\#$ 3.3 and $F\#$ 2.8, respectively designed using (2), and the effective frequency responses ($R_i(\omega, \nu)$, $i = 1, 2, 3$) of the composite FIR filters constructed using the set of nested component filters. When the aperture is set to $F\#$ 4.3, the two outer component filters are turned off and only the 7×7 center filter is applied. This provides considerable power consumption efficiency in hardware when in the $F\#$ 4.3 aperture setting. At $F\#$ 2.8, all three components filters are used. As shown in Fig. 4, the composite FIR filter responses using the filter bank are nearly identical to those of the FIR Wiener filters, but requiring significantly less computational resources.

Fig. 5 shows the simulated images before and after applying the optimized composite FIR filters shown in Fig. 4

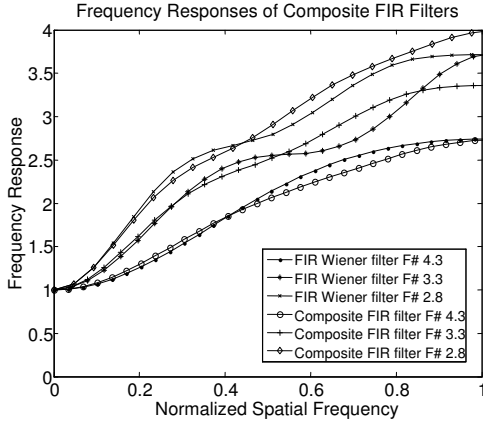


Fig. 4. The diagram shows the composite FIR filter responses for three f-numbers. The composite FIR filters achieve nearly identical performance to the FIR Wiener filters.

for the three f-number settings. The significant difference of the optical blur for different f-numbers can be observed in the top row of Fig. 5, and correspondingly, the images restored by the optimized composite filters are shown in the bottom row, where all three processed images exhibit significantly improved sharpness at the same level.

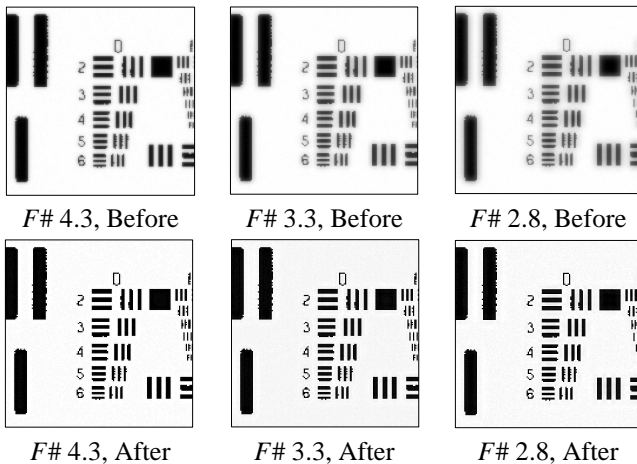


Fig. 5. The diagram shows simulated results with the images before and after being processed by the composite FIR filters for three f-numbers.

Table 1 compares the MSE values for the FIR Wiener filters separately designed for the three f-numbers, the composite FIR filters comprised of the optimized filter bank kernels, and the single IIR Wiener filter optimized for the three f-numbers. The table shows that the MSEs of the composite FIR filters are very close to the separately designed FIR Wiener filters, whereas the single IIR Wiener filter produces slightly lower MSE than the composite FIR filter for $F\# 3.3$ and significantly higher MSEs for the other two f-numbers.

Table 1. MSE values produced by different filtering approaches for three f-numbers.

| | F# 4.3 | F# 3.3 | F# 2.8 |
|------------------------------------|---------------|---------------|---------------|
| Separate FIR Wiener filters | 6.5E-5 | 9.9E-5 | 1.6E-4 |
| Composite FIR filters | 9.4E-5 | 1.7E-4 | 1.8E-4 |
| Single IIR Wiener filter | 1.5E-3 | 1.6E-4 | 1.2E-3 |

4. CONCLUSIONS

We have presented a low-complexity filter bank approach to compensate for aberrations resulting from different f-numbers in a jointly designed electro-optical imaging system. We apply our approach to the example of a strongly aberrated optical system having variable f-numbers. We demonstrate the effectiveness of our approach by showing that the composite FIR filters achieve the nearly identical performance to the separately designed FIR Wiener filters for each f-number, while requiring significantly less computational resources in hardware than the naive approach. It is, however, beyond the scope of this paper to evaluate the hardware complexity for the proposed approach in detail.

5. REFERENCES

- [1] Edward Dowski and W. Thomas Cathey, "Extended depth of field through wave-front coding," *Applied Optics*, vol. 41, pp. 1859–1866, 1995.
- [2] Nicholas George and Wanli Chi, "Extended depth of field using a logarithmic asphere," *Journal of Optics A: Pure Applied Optics*, vol. 5, no. 5, pp. S157–S163, 2003.
- [3] Pantazis Mouroulis, "Depth of field extension with spherical optics," *Optics Express*, vol. 16, no. 17, pp. 12995–13004, 2008.
- [4] David G. Stork and M. Dirk Robinson, "Theoretical foundations for joint digital-optical analysis of electro-optical imaging systems," *Applied Optics*, April 2008.
- [5] Robert E. Fischer and Biljana Tadic-Galeb, *Optical System Design*, McGraw-Hill, New York, 2000.
- [6] Anil K. Jain, *Fundamentals of Digital Image Processing*, Prentice Hall, Englewood Cliffs, New Jersey, 1st edition, 1989.
- [7] J.C. Lagarias and J. A. Reeds and M. H. Wright and P. E. Wright, "Convergence properties of the nelder-mead simplex method in low dimensions," *SIAM Journal of Optimization*, vol. 9, no. 1, pp. 112–147, 1998.